Nanoscale and Microscale Thermophysical Engineering, 10: 321–331, 2006

ISSN: 1556-7265 print / 1556-7273 online
DOI: 10.1080/15567260601009171

THERMAL PROPERTIES AND LATTICE DYNAMICS OF POLYCRYSTALLINE MFI ZEOLITE FILMS

A.M. Greenstein and S. Graham
Woodruff School of Mechanical Engineering, Georgia Institute of Technology, Atlanta, Georgia

Y.C. Hudiono and S. Nair
School of Chemical & Biomolecular Engineering, Georgia Institute of Technology, Atlanta, Georgia

A study of the thermal properties of the zeolite MFI by a combination of experimental measurements and lattice dynamical modeling is presented. Thermal conductivity data in the range of 150–400 K was obtained through 3ω measurements on polycrystalline zeolite films. While Debye theory is inadequate in predicting the zeolite thermal properties, a detailed calculation of the specific heat using a full set of dispersion relations obtained from atomistic simulations gives excellent agreement with experiments. In addition, the thermal conductivity is successfully reproduced by a phonon relaxation time–based model. The results indicate the possibility of developing a predictive model of the thermal properties of complex zeolite materials.

KEY WORDS: nanoporous materials, zeolites, thermal properties, lattice dynamics

INTRODUCTION

Zeolites (nanoporous crystalline aluminosilicates) have a wide range of applications as catalysts, molecular sieves for chemical separations and sensing, low-k dielectrics, and ordered templates for nanotechnological materials [1–3]. In recent years, they are being increasingly considered for applications in which heat transfer plays an important role. The use of sorption-based heat exchange either in a standalone or hybrid mode may offer solutions to heat transfer problems in large-scale ($>$1 kW) heat recovery and cooling [4, 5], as well as in cooling small-scale ($<$100 W) microelectronic devices [6]. Their potential applications as low-k dielectric materials [7] also necessitate knowledge of their thermophysical properties.

Zeolite materials exist in over 200 crystal structures with varied and sometimes anomalous (e.g., negative thermal expansion [8, 9]) thermophysical properties [10]. Despite their growing importance in modern heat transfer applications, there are still few reports [10, 11] of their thermal properties. The specific heat and thermal

Received 15 September 2005; accepted 5 December 2005.
The authors thank Professor Brandon Olson of the Aerospace and Mechanical Engineering Department at the University of Oklahoma for his helpful discussions on 3ω measurements and data analysis codes.
Address correspondence to S. Graham, Woodruff School of Mechanical Engineering, Georgia Institute of Technology, 801 Ferst Drive NW, Atlanta, GA 30332. E-mail: sgraham@me.gatech.edu

conductivity are usually measured by compacting the zeolite powder into a disk and using a model of the composite to extract the intrinsic properties from calorimetric or heat flux data. A computational approach for determining thermal properties of zeolite materials relies on molecular dynamics (MD) simulations using atomistic force fields. However, this is a difficult task [12] owing to the generally slow convergence of the computed heat flux. At temperatures for which the system can be well described by classical mechanics, equilibrium MD methods can predict the (classical) specific heat with good accuracy. Computation of thermal conductivity is possible, but more difficult, using equilibrium or nonequilibrium MD methods [10, 13]. In addition, the lack of comprehensive experimental data complicates interpretation of simulated thermal properties.

In the case of thermal conductivity, another crucial aspect is the description of phonon scattering processes that determine the rate of heat transfer in a material. The solution of the generalized Boltzmann phonon transport equation is often undertaken with a "relaxation time" approach to account for phonon scattering processes [14]. Theoretically, relaxation times can be obtained directly from the Fermi golden rule [15] if full details of the phonon dispersion and mode eigenvectors can be calculated. Difficulties in directly calculating relaxation times have led to various simplifying assumptions for incorporating the effects of different scattering mechanisms on phonon transport. Good agreement is obtained with experimental data for crystals with only a small number of phonon branches (e.g., Si, Ge, diamond). However, these fitted relaxation parameters are expected to be inadequate for complex crystals such as zeolites.

In this article, we present a generalized modeling framework along with experimental data to describe the thermal properties of complex crystalline materials such as zeolites. Two main challenges in the thermophysics of zeolite materials are: (a) development of methods and samples for accurate thermal property measurements, and (b) generalization of thermophysical property theories [16, 17] to complex, low-symmetry zeolite crystals containing hundreds of atoms in a unit cell. In this study, we have chosen the zeolite MFI [18] as a well-characterized model system. MFI is a zeolite with ordered sinusoidal and straight channels of a nominal pore size $\sim$0.6 nm, running along the *a*- and *b*- directions, respectively (Figure 1). Polycrystalline MFI films of different crystal orientations and microstructures can be synthesized by the technique of "seeded hydrothermal growth," described elsewhere [19]. The ability to grow dense, polycrystalline films (1–50 μm) on surfaces such as silicon and glass allows us to apply 3ω measurement techniques that employ microfabricated elements deposited on the surface to provide thermal excitation of the thin film and measurement of the sample response. We then show that detailed calculations of the specific heat based on phonon dispersion curves give excellent agreement with experiments. We use a highly accurate atomistic force field to calculate the phonon dispersion curves. This approach has attractive aspects that complement MD simulations, since we can calculate the dispersion with high accuracy and less computational effort and physically analyze the results in reciprocal space, whereas the use of a similarly accurate force field in MD could considerably increase the simulation time and data analysis effort if accurate thermal property predictions are desired. Finally, an approach is outlined for calculating the thermal conductivity and is supported with preliminary calculations.

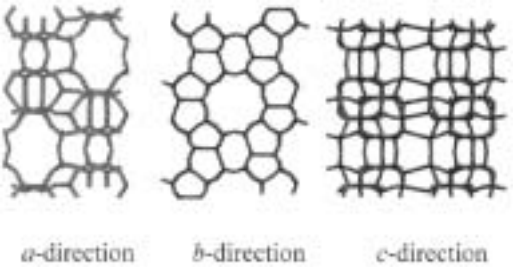

Figure 1. Structure of zeolite MFI viewed down *a*-, *b*-, and *c*-axes respectively.

EXPERIMENTAL

Preparation of MFI Polycrystalline Films

Silicon wafers were cleaned as described in Boudreau et al. [20]. A colloidal suspension of silicalite (SiO_2) MFI nanocrystals ($\sim$100 nm) were prepared as reported in Oh and Nair [21]. A 50% suspension in ethanol was filtered, ultrasonicated, and spin-coated (Model 100CB, Brewer Science, Inc.) on the silicon substrate at 3000 rpm for 30 s. The coated substrates were dried at 60°C overnight. Silicalite (SiO_2) MFI films were then grown in a Teflon-lined stainless steel autoclave by secondary growth of the nanocrystals at 175°C for 48 h, with a growth solution composition as described elsewhere [19]. The films were rinsed with hot DI water, dried at 60°C overnight, and then polished with SiC paper (Buehler Inc., 1200 and 4000 grit) at 100 rpm for 15 and 35 s, respectively. Calcination in air (500°C, 5 h) removes the organic tetrapropylammonium (TPA) template, creating an empty nanopore structure. Both calcined and uncalcined MFI films were prepared. The samples were characterized by SEM (Hitachi X800, 10kV) and X-ray diffraction (PANalytical X'Pert Pro, Cu Kα).

Thermal Property Measurements

The thermal properties were determined using the 3ω technique, in which an aluminum metal line is used as a heater and a thermometer [19]. An aluminum line heater of approximately 250 nm thickness and 75 μm width was directly deposited onto the MFI surface. Both the in-phase and out-of-phase components of the third harmonic voltage drop were utilized over a broad band frequency range (90–2000 Hz) in order to deduce the thermal conductivity through the film thickness. Details of the analysis algorithm can be found elsewhere [22]. The use of this frequency range corresponded to a thermal penetration depth that remained in the zeolite film, eliminating contributions from the substrate. The measurements were performed at temperatures between 150 and 400 K in an evacuated cryostat to control convective heat losses.

RESULTS AND DISCUSSION

MFI Film Synthesis and Thermal Property Measurements

The MFI crystals in the film have a (002) out-of-plane orientation as was determined by X-ray diffraction. Figure 2a shows the SEM cross section and top

views of the ~30 μm thin film. The facets represent the (101) planes of the crystals [19] and increase the surface roughness, resulting in a poor quality of line heater deposition. The top view shows the surface of the film with a grain size of 4 μm. Figure 2b shows the membrane after polishing. The thickness was reduced to ~20 μm and the surface is considerably smoother, allowing a reliable heater deposition.

Figures 3 and 4 show the thermal conductivity and specific heat data, respectively, over the temperature range of 150–400 K. Specific heat data were measured using differential scanning calorimetry and taken from the literature [8], and thermal conductivity was measured by the authors. The thermal conductivity (experimental and model-fitted) for MFI is of the same order of magnitude as that previously reported for zeolites FAU and LTA by MD simulation [10, 13] and by experiment [11, 23]. Calcined MFI exhibits a thermal conductivity between 0.8 and 1 W/m/K in this temperature range, whereas the uncalcined MFI (containing the TPA cations) shows a considerably higher conductivity (1–1.5 W/m/K). Qualitatively, this can be attributed to a more efficient transfer of phonon energy in the denser uncalcined material (the calcined and uncalcined MFI film densities are 1793 and 2115 kg/m^3, respectively). In addition, the temperature dependence of thermal conductivity appears to be dominated by the strong contribution of specific heat of MFI and not as much by phonon-phonon scattering events in the large zeolite crystals.

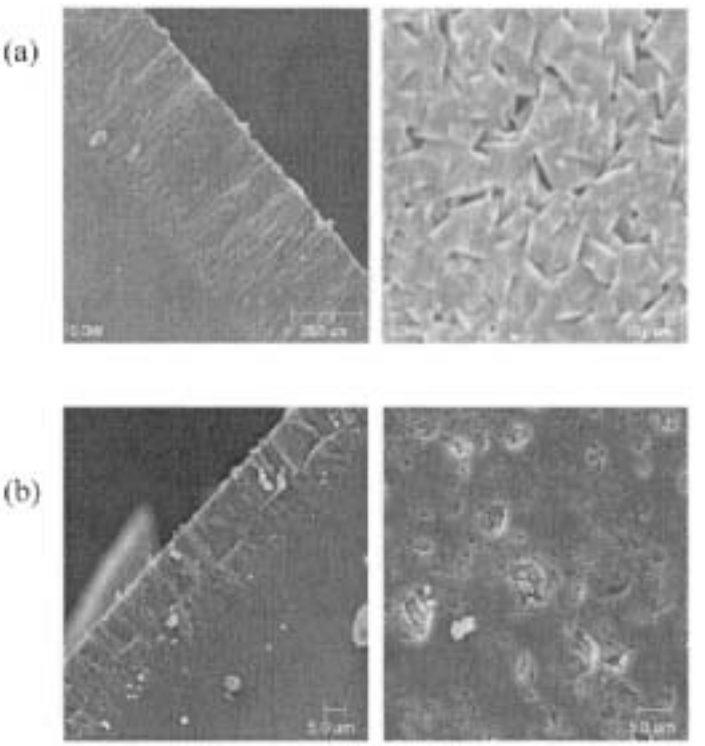

Figure 2. SEM images (left: cross section, right: top view) of (a) as-synthesized, and (b) polished MFI films.

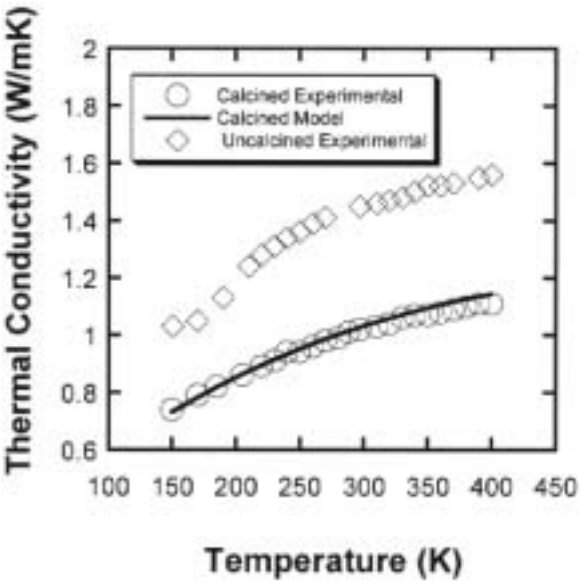

Figure 3. Thermal conductivity data measured by the 3ω method for calcined and uncalcined MFI, and the model proediction for conductivity of calcined MFI.

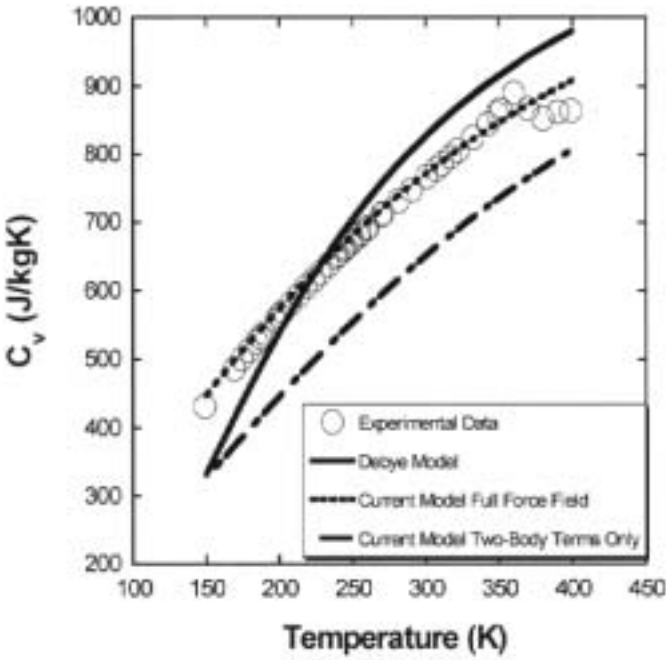

Figure 4. Specific heat of calcined MFI. Experimental data are from Boerio-Goates et al. [34].

Thermal Property Calculations

Traditionally, specific heat is modeled *via* Debye theory, which uses the Debye temperature [23]. The Debye temperature is often obtained by fitting the Debye model to specific heat data. An attempt to fit the Debye model to MFI (Figure 4) shows that it is unable to predict the specific heat of MFI. The theory makes several assumptions: (1) only the three acoustic phonon branches contribute to the specific heat, (2) the summation over discrete phonon states can be replaced by an integral, (3) the phonon dispersion is linear and is the same for all polarizations, (4) the dispersion is isotropic, and (5) there is a cutoff frequency represented by the Debye temperature [23]. MFI, an anisotropic orthorhombic crystal, has 288 atoms per unit cell, 864 dispersion branches, and no appreciable band gap between the 3 acoustic and 861 optic modes of nonlinear dispersion. Hence, all the above assumptions but (2) are invalid.
A general expression for the specific heat is [24]:

$$C_v = k_B \sum_P \sum_{\vec{K}} x_P\left(\vec{K}\right)^2 \frac{e^{x_{P(\vec{K})}}}{\left(e^{x_P(\vec{K})} - 1\right)^2}$$
$$x_P\left(\vec{K}\right) = \left(\frac{\hbar\omega_P\left(\vec{K}\right)}{k_B T}\right) \tag{1}$$

The outer summation is over all 864 polarizations. The inner summation is over all phonon modes or wave vectors in the first Brillouin zone. The assumptions we make are that the wave vectors are continuous, the dispersion curves are temperature independent, anharmonicity can be neglected, and thermal energy storage occurs only in phonons. Replacing the summation over the wave vectors with an integral over the first Brillouin zone results in:

$$C_v = k_B \frac{V}{(2\pi)^3} \sum_{P=1}^{864} \int\int\int x_P\left(\vec{K}\right)^2 \frac{e^{x_P(\vec{K})}}{\left(e^{x_P(\vec{X})} - 1\right)^2} dV_{BZ} \tag{2}$$

To obtain the specific heat with Eq. (2), the dispersion curves must be calculated in all directions. The General Utility Lattice Program (GULP) [25] was used to calculate phonon properties with two different force fields. The first [26] is a two-body force field that uses only a Buckingham potential and Coulomb potential. The second includes a Buckingham potential, a Coulomb potential, a three-body bending term, and a core-shell model for oxygen polarizability [27].

A unique discretization scheme is used to integrate over the box-shaped Brillouin zone, which is consistent with the orthorhombic unit cell for MFI. Due to symmetry considerations, the calculation need only be performed in the positive octant. In this scheme, the three orthogonal faces in the positive octant are discretized into 4 subsections, giving a total of 12 subsections. The volume of each subsection is bounded by lines from the edges of the subsection's face on the Brillouin zone surface to the origin. Figure 5 shows a schematic of the Brillouin zone discretization. Dispersion curves are calculated from the origin to the center of each subsection. It is assumed that in a given subsection, each dispersion curve is dependent only on k_x, k_y, or k_z, depending on whether the subsection ends on the k_x, k_y, or k_z plane. The final expression for C_v is:

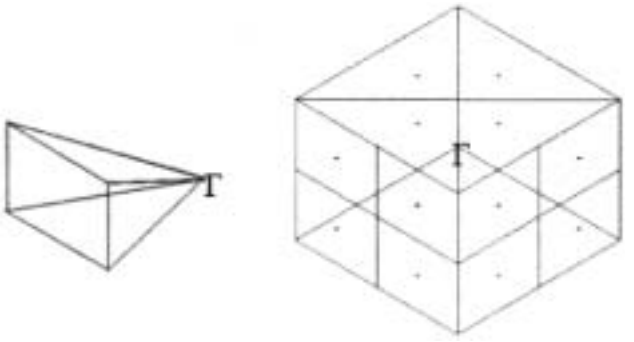

Figure 5. Schematic showing full volume of one of the twelve subsections, and the positive octant of the Brillouin zone of MFI. For clarity, divisions between subsections and centers of subsections are marked only on Brillouin zone surface.

$$C_v = \frac{k_B}{\pi^3 \rho} \sum_{i=1}^{3} \sum_{S=1}^{4} \sum_{P=1}^{864} \int\int\int x_P\left(\vec{K}\right)^2 \frac{e^{x_P\left(\vec{K}\right)}}{\left(e^{x_P\left(\vec{K}\right)} - 1\right)^2} dV_{BZ,j}$$

$$dV_{BZ1} = \frac{K_x^2}{\cos^3\theta \sin^2\phi} dK_x d\phi d\theta$$

$$dV_{BZ2} = \frac{K_y^2}{\sin^3\theta \sin^2\phi} dK_y d\phi d\theta \tag{3}$$

$$dV_{BZ3} = \frac{K_z^2}{\cos^3\phi} \sin\phi dK_z d\phi d\theta$$

The integration is over the volume elements $dV_{BZ,i}$. The i summation is over the 3 faces and the S summation is for the 4 discretized subsections that end on each face. With appropriate geometric adjustments, this model can be used to predict the heat capacity of many crystalline dielectrics and semiconductors.

We first test the computational technique with silicon, modeled using the well-established Stillinger-Weber potential [28]. Equation (3) is used, but the differential volume elements of the sections of the FCC Brillouin zone are redefined and discretized in the appropriate manner to yield:

$$dV_{BZi} = K_i^2 \sin\phi \alpha_i^{3/2} dK_i d\phi d\theta$$

where

$$\alpha_1 = \left(1 - \frac{K_2}{K_1} + \frac{K_3}{K_1}\right)^2 + \left(1 + \frac{K_2}{K_1} - \frac{K_3}{K_1}\right)^2 + \left(1 - \frac{K_2}{K_1} + \frac{K_3}{K_1}\right)^2,$$

$$\alpha_2 = \left(\frac{K_1}{K_2} - 1 + \frac{K_3}{K_2}\right)^2 + \left(\frac{K_1}{K_2} + 1 - \frac{K_3}{K_2}\right)^2 + \left(-\frac{K_1}{K_2} + 1 + \frac{K_3}{K_2}\right)^2,$$

$$\alpha_3 = \left(\frac{K_1}{K_3} - \frac{K_2}{K_3} + 1\right)^2 + \left(\frac{K_1}{K_3} + \frac{K_2}{K_3} - 1\right)^2 + \left(-\frac{K_1}{K_3} + \frac{K_1}{K_3} + 1\right)^2,$$

and

$$\frac{K_1}{K_2} = \frac{\cos\theta + \sin\theta}{\sin\theta + \cot\phi}, \quad \frac{K_1}{K_3} = \frac{\cos\theta + \sin\theta}{\cos\theta + \cot\phi}, \quad \frac{K_2}{K_3} = \frac{\sin\theta + \cot\phi}{\cos\theta + \cot\phi} \tag{4}$$

The results of the specific heat model are shown in Figure 6. At high temperatures both the current model and Debye model converge to the Dulong-Petit limit. The discrepancy between experiment and the model at higher temperatures could be caused by (1) the omission of the electronic contribution to the specific heat, (2) the assumption that the lattice binding energy is constant with temperature, (3) numerical error introduced in the integration scheme, (4) any inherent limitations of the Stillinger-Weber potential, or (5) anharmonic and temperature-dependent effects.

Electronic contributions can be ruled out in this temperature range, since the free electron concentration at 350 K is $\sim 10^{11}$ cm^{-3} and is not enough to make a significant contribution to the specific heat. The lattice energy was calculated using lattice constants at different temperatures with the Stillinger-Weber potential; the lattice specific heat was found to be negligible. To investigate the quality of the interatomic potential and integration scheme, comparison with a quantum mechanical plane-wave calculation using a Brillouin zone sample method rather than integration [29] resulted in nearly identical results. Thus, neither the effective potential nor the integration scheme used in the current approach is believed to be the cause of the deviations from the experiment. Anharmonic effects can result from changes in lattice constant with temperature, or limitations inherent in treating phonons as a non-interacting boson gas. To address the former type of anharmonic effects, phonon spectra were calculated using experimentally measured lattice constants at different temperatures; it was found that thermal expansion had negligible effects on the phonon frequencies. We believe that discrepancies from experiment result from the latter type of anharmonic effects, which are not addressed because the phonons are modeled as a non-interacting boson gas.

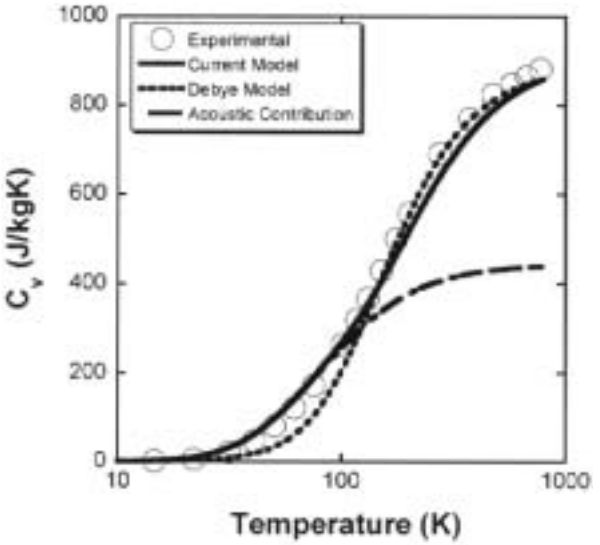

Figure 6. Specific heat of silicon. Experimental data is from Touloukian and Buyco [35].

Next, the model was applied to calculate the specific heat of MFI. Figure 4 shows good agreement between the current model and experiment when an accurate force field is used. The only deviation of the current model from experiment is in the region around 350 K. This is most likely due to the well-known displacive second-order phase transition of MFI in this temperature region [9, 30]. In the present study, we have only used the low-temperature crystal structure and hence the effects of the phase transition are not captured. However, this can be addressed computationally within the framework of free energy minimization techniques, as shown recently [31]. In other words, the free energy of the crystal could first be minimized at each temperature to capture potential phase transitions, before calculating the phonon properties. Neither the two-body force field (even when used with the current model) nor the Debye model produces accurate results. At 400 K the specific heat is still increasing strongly with temperature. This is because the Dulong-Petit law is not approached for this structure until 1200–1300 K. The temperature at which the Dulong-Petit limit is reached is directly dependent on the highest phonon frequencies that exist in the solid. The highest phonon frequency in MFI ($\sim$30 THz) is nearly double that of silicon.

Using the current theoretical approach, the thermal conductivity can be derived as [23]:

$$k_j = \frac{k_B}{\pi^3} \sum_{i=1}^{3} \sum_{S=1}^{4} \sum_{P=1}^{288\times 3} \int\int\int x_P(\bar{K})^2 \frac{e^{x_P(\bar{K})}}{\left(e^{x_P(\bar{K})}-1\right)^2} v_{PS,j}^2(K_i)\tau_{PS,j}(K_i)dV_{BZ,i} \qquad (5)$$

The j index runs over the three principal crystal directions. The conductivity is strongly influenced by phonon velocities (v) and their scattering rates (quantified by phonon relaxation times τ). Despite the use of fitted parameters, widely used relaxation time expressions [14, 32] are unable to reproduce the thermal conductivity of MFI, which requires more detailed quantification of the scattering processes. However, we found that in MFI the conductivity can be reproduced by Eq. (5) with a single relaxation time parameter for all phonons. All other quantities are obtained from the calculation of phonon dispersion. This result is shown in Figures 3 for the c direction of MFI which corresponds to the out-of-plane orientation of the films studied here.

The value of the fitted relaxation time in our thermal conductivity calculations was 9.2 ps, which is the same order of magnitude as those estimated for quartz near room temperature (250 K) [33]. The estimates in previous works were obtained by decomposition of MD-derived heat flux autocorrelation functions. Therefore, the fitted "effective" relaxation time for MFI appears reasonable. From the dispersion calculations, the average phonon velocity in MFI is estimated at approximately 500 m/s at 300 K. Thus, the low thermal conductivity is due in part to the low phonon velocity. Based on the fitted relaxation time, the phonon mean free path was found to be 4.5 nm at 300 K. Despite its low conductivity, MFI cannot be modeled as an amorphous material. Attempts to model it using a minimum thermal conductivity model, wherein the modal relaxation times were calculated as half the period of the phonons of that mode, resulted in a drastic underestimation of the conductivity.

CONCLUSIONS

The agreement between the current model and experiment creates justifiable optimism that the thermal properties of complex materials like MFI can be predicted

ab initio with low or moderate computational expense. This has been demonstrated in the current study for the specific heat. For thermal conductivity, the good quality of the single-parameter fit indicates that a detailed calculation of scattering rates can allow a completely predictive model. While the detailed phonon dispersion relationships may be obtained using the outlined approach, work remains to be done in efficiently determining the relaxation time parameters analytically or semi-analytically from Fermi's golden rule or molecular dynamics simulations. The adaptation of the present technique to other complex zeolites should yield useful thermophysical properties and more detailed insight into the dependence of phonon transport and scattering mechanisms on the zeolite structure and composition.

REFERENCES

1. M.E. Davis, Ordered Porous Materials for Emerging Applications, *Nature*, vol. 417, pp. 813–821, 2002.
2. Z.P. Lai, G. Bonilla, I. Diaz, J.G. Nery, K. Sujaoti, M.A. Amat, E. Kokkoli, O. Terasaki, R.W. Thompson, M. Tsapatsis, and D.G. Vlachos, Microstructural Optimization of a Zeolite Membrane for Organic Vapor Separation, *Science*, vol. 300, pp. 456–460, 2003.
3. K. Mukhopadhyay, A. Koshio, N. Tanaka, and H. Shinohara, A Simple and Novel Way to Synthesize Aligned Nanotube Bundles at Low Temperature, *Japanese Journal of Applied Physics Part 2—Letters*. vol. 37, pp. L1257–L1259, 1998.
4. A.O. Dieng and R.Z. Wang, Literature Review on Solar Adsorption Technologies for Ice-Making and Air-Conditioning Purposes and Recent Developments in Solar Technology, *Renewable & Sustainable Energy Reviews*, vol. 5, pp. 313–342, 2001.
5. M. Tatlier and A. Erdem-Senatalar, The Performance Analysis of a Solar Adsorption Heat Pump Utilizing Zeolite Coatings on Metal Supports, *Chemical Engineering Communications*, vol. 180, pp. 169–185, 2000.
6. J.M. Gordon, K.C. Ng, H.T. Chua, and A. Chakraborty, The Electro-Adsorption Chiller: A Miniaturized Cooling Cycle with Applications to Micro-Electronics, *International Journal of Refrigeration-Revue Internationale Du Froid*, vol. 25, pp. 1025–1033, 2002.
7. Z.B. Wang, H.T. Wang, A. Mitra, L.M. Huang, and Y.S. Yan, Pure-Silica Zeolite Low-k Dielectric Thin Films, *Advanced Materials*, vol. 13, pp. 746–749, 2001.
8. J. Boerio-Goates, R. Stevens, B. Lang, and B.F. Woodfield, Heat Capacity Calorimetry—Detection of Low Frequency Modes in Solids and an Application to Negative Thermal Expansion Materials, *Journal of Thermal Analysis and Calorimetry*, vol. 69, pp. 773–783, 2002.
9. S.H. Park, R.W.G. Kunstleve, H. Graetseh, and H. Gies, The Thermal Expansion of the Zeolites MFI, AFI, DOH, DDR, and MTN in Their Calcined and as Synthesized Forms, *Progress in Zeolite and Microporous Materials, Pts A-C*, vol. 105, pp. 1989–1994, 1997.
10. V.V. Murashov, Thermal Conductivity of Model Zeolites: Molecular Dynamies Simulation Study, *Journal of Physics—Condensed Matter*, vol. 11, pp. 1261–1271, 1999.
11. V.V. Murashov and M.A. White, Thermal Properties of Zeolites: Effective Thermal Conductivity of Dehydrated Powdered Zeolite 4A, *Materials Chemistry and Physics*, vol. 75, pp. 178–180, 2002.
12. P.K. Schelling, S.R. Phillpot, and P. Keblinski, Comparison of Atomic-Level Simulation Methods for Computing Thermal Conductivity, *Physical Review B*, vol. 65, art. 144306, 2002.
13. A.J.H. McGaughey and M. Kaviany, Thermal Conductivity Decomposition and Analysis Using Molecular Dynamies Simulations—Part II. Complex Silica Structures, *International Journal of Heat and Mass Transfer*, vol. 47, pp. 1799–1816, 2004.
14. J. Callaway, Low-Temperature Lattice Thermal Conductivity, *Physical Review*, vol. 122, p. 787, 1961.

15. G.P. Srivastava, *The Physics of Phonons*, Adam Hilger, Bristol, UK, 1990.
16. M.G. Holland, Analysis of Lattice Thermal Conductivity, *Physical Review*, vol. 132, p. 2461, 1963.
17. D.T. Morelli, J.P. Heremans, and G.A. Slack, Estimation of the Isotope Effect on the Lattice Thermal Conductivity of Group IV and Group III–V Semiconductors, *Physical Review B*, vol. 66, art. 195304, 2002.
18. W.M. Meier, D. Olson, C. Baerlocher, and International Zeolite Association, Structure Commission, *Atlas of Zeolite Structure Types*, 4th Rev. ed., Elsevier, New York, 1996.
19. G. Xomeritakis, A. Gouzinis, S. Nair, T. Okubo, M.Y. He, R.M. Overney, and M. Tsapatsis, Growth, Microstructure, and Permeation Properties of Supported Zeolite (MFI) Films and Membranes Prepared by Secondary Growth, *Chemical Engineering Science*, vol. 54, pp. 3521–3531, 1999.
20. L.C. Boudreau, J.A. Kuck, and M. Tsapatsis, Deposition of Oriented Zeolite A Films: In Situ and Secondary Growth, *Journal of Membrane Science*, vol. 152, pp. 41–59, 1999.
21. W. Oh and S. Nair, Concentration Profiling of a Molecular Sieve Membrane by Step-Scan Photoacoustic Spectroscopy, *Journal of Physical Chemistry B*, vol. 108, pp. 8766–8769, 2004.
22. B. Olson, S. Graham, and K. Chen, A Practical Extension of the 3 Omega Method to Multilayer Structures, *Review of Scientific Instruments*, vol. 76, art. 053901, 2005.
23. C. Kittel, *Introduction to Solid State Physics*, 7th ed., John Wiley & Sons, New York, 1996.
24. C. Kittel and H. Kroemer, *Thermal Physics*, 2nd ed., W.H. Freeman Company, New York, 1980.
25. J.D. Gale, GULP: A Computer Program for the Symmetry-Adapted Simulation of Solids, *Journal of the Chemical Society—Faraday Transactions*, vol. 93, pp. 629–637, 1997.
26. G.J. Kramer, N.P. Farragher, B.W.H. van Beest, and R.A. van Santen, Interatomic Force-Fields for Silicas, Aluminophosphates, and Zeolites—Derivation Based on Abinitio Calculations, *Physical Review B*, vol. 43, pp. 5068–5080, 1991.
27. M.J. Sanders, M. Leslie, and C.R.A. Catlow, Interatomic Potentials for SiO_2, *Journal of the Chemical Society—Chemical Communications*, vol. 19, pp. 1271–1273, 1984.
28. F.H. Stillinger and T.A. Weber, Computer-Simulation of Local Order in Condensed Phases of Silicon, *Physical Review B*, vol. 31, pp. 5262–5271, 1985.
29. S.Q. Wei, C.L. Li, and M.Y. Chou, Ab-Initio Calculation of Thermodynamic Properties of Silicon, *Physical Review B*, vol. 50, pp. 14587–14590, 1994.
30. D.G. Hay and H. Jaeger, Orthorhombic Monoclinic Phase-Changes in ZSM-5 Zeolite Silicalite, *Journal of the Chemical Society—Chemical Communications*, vol. 21, pp. 1433–1433, 1984.
31. R. Grau-Crespo, E. Acuay, and R.R. Ruiz-Salvador, A Free Energy Minimisation Study of the Monoclinic-Orthorhombic Transition in MFI Zeolite, *Chemical Communications*, vol. 21, pp. 2544–2545, 2002.
32. P.G. Klemens, Thermal Conductivity and Lattice Vibrational Modes, *Solid State Physics—Advances in Research and Applications*, vol. 7, pp. 1–98, 1958.
33. A.J.H. McGaughey and M. Kaviany, Molecular Dynamics Calculations of the Thermal Conductivity of Silica Based Crystals, 8th AIAA/ASME Joint Thermophysics and Heat Transfer Conference, S. Louis, Missouri, June 2002.
34. J. Boerio-Goates, R. Stevens, B.K. Hom, B.F. Woodfield, P.M. Piecione, M.E. Davis, and A. Navrotsky, Heat Capacities, Third-Law Entropies and Thermodynamic Functions of SiO_2 Molecular Sieves from $T = 0$ K to 400 K, *Journal of Chemical Thermodynamics*, vol. 34, pp. 205–227, 2002.
35. Y.S. Touloukian and E.H. Buyco, *Thermophysical Properties of Matter*, vol. 4 IFI/Plenum, New York, 1970.